RAL-93-077

Science and Engineering Research Council
Rutherford Appleton Laboratory
Chilton DIDCOT Oxon OX11 0QX

RAL-93-077

MRS Parton Distributions

A D Martin W J Stirling and R G Roberts

November 1993

RAL-93-077
DTP/93/86
October 1993

MRS Parton Distributions*

A.D. Martin and W.J. Stirling

Department of Physics, University of Durham
Durham DH1 3LE, England

and

R.G. Roberts

Rutherford Appleton Laboratory,
Chilton, Didcot OX11 0QX, England

Abstract

The MRS parton distribution analysis is described. The latest sets are shown to give an excellent description of a wide range of deep-inelastic and other hard scattering data. Two important theoretical issues—the behaviour of the distributions at small x and the flavour structure of the quark sea—are discussed in detail. A comparison with the new structure function data from HERA is made, and the outlook for the future is discussed.

*Based on talks presented by W.J. Stirling at the Workshop on Quantum Field Theoretical Aspects of High Energy Physics, Kyffhäuser, and at the Topical Meeting on QCD at HERA, DESY

1 Introduction

The parton distribution functions $f_{i/p}(x,Q^2)$ $(i = u,d,s,\ldots,g)$ describe how the proton's momentum is shared between its quark and gluon constituents, when probed at length scale Q^{-1}. They are directly related to the structure functions $F_i(x,Q^2)$ measured in lepton-nucleon deep-inelastic scattering (DIS) experiments. There are two main reasons—one experimental and one theoretical—why these distributions are important. First, a detailed knowledge of parton distributions is necessary in order to make precise calculations of 'hard scattering' cross sections at current and future hadron-hadron colliders. Second, the parton structure is interesting in its own right, providing tests of perturbative QCD and insight into the non-perturbative long-distance structure of hadrons. For example, novel perturbative QCD effects are expected to become apparent at small x ($\lesssim 10^{-3}$), where soft gluon emission off the incoming parton leads to a power series in $\alpha_s \log(1/x)$. Resummation of this series, via the Lipatov (or BFKL) equation [1], gives a gluon distribution which behaves as

$$xf_g \sim x^{-\lambda} \tag{1}$$

as $x \to 0$, with λ predicted, typically, to be about 0.5. Parton distributions also reveal how SU(3) flavour symmetry is broken in the quark-antiquark sea, which has important implications for non-perturbative models of the structure of hadrons.

There is a long history of determining parton distributions from data on deep-inelastic and other hard-scattering processes. In this review we will describe the 'MRS' series of distributions, which have provided some of the most accurate, up-to-date information on parton structure, making full use of the ever-increasing precision of the experimental measurements. Although broadly similar to other 'modern' sets of distributions, the MRS distributions do differ in some important respects. In what follows we shall, where appropriate, draw attention to these differences.

Table 1 lists the MRS sets of recent years, together with the data fitted.[†] The original sets MRS(1,2,3) were constrained mainly by DIS data from EMC. When these data were found to be in disagreement with new BCDMS data[8], two new sets HMRS(E,B) were provided. With the advent of data from NMC, this discrepancy was resolved in favour of the BCDMS-type fits. The KMRS sets explored the small-x behaviour of the distributions with the B_ set incorporating, for the first time, the Lipatov behaviour $xg, xq \sim x^{-0.5}$ as $x \to 0$. The most significant recent (pre-HERA) experimental developments were the new NMC measurements [9] of $F_2^{\mu p}$ and $F_2^{\mu n}$ (from $F_2^{\mu D}$) and the CCFR measurements [10] of $F_2^{\nu N}$ and $xF_3^{\nu N}$. These provided the first detailed information on quark distributions in the $0.01 \lesssim x \lesssim 0.1$ range . The KMRS sets (and almost all others) considerably underestimated the structure functions in this region, see Fig. 1. The 1992 MRS(S_0,D_0,D_-) sets incorporated these new data. A new feature was the provision for the first time of light quark flavour asymmetry in the sea, *i.e.* $\bar{u} \neq \bar{d}$, motivated by the NMC measurements [11] of the Gottfried Sum Rule (see below). When the NMC and CCFR data were finally published, the fits were fine-tuned, resulting in the most recent MRS(S_0',D_0',D_-') sets.

[†]The **FORTRAN** code for all of these can be found, for example, in the PDFLIB compilation [2]

set	μ-DIS	ν-DIS	Prompt γ	D-Yan	W, Z
MRS '88 [3] (sets 1,2,3)	EMC + ...	CDHSW	AFS ($+J/\psi$)	—	—
HMRS '90 [4] (sets E,B)	EMC BCDMS NMC(n/p)	CDHSW	WA70	E605	—
KMRS '90 [5] (sets B_0,B_-)	BCDMS NMC(n/p)	CDHSW	WA70	E605	—
MRS (Apr '92) [6] (sets D_0,D_-)	BCDMS NMC(p,n)†	CDHSW CCFR†	WA70	E605	(UA2, CDF
MRS (Nov '92) [7] (sets D'_0,D'_-)	BCDMS NMC(p,n)	CCFR	WA70	E605	(UA2, CDF)

Table 1: MRS parton distributions together with the data used in the various analyses. Data marked † were used in preliminary form.

Deep-inelastic muon and neutrino data tightly constrain the valence and sea quark distributions. In contrast, the gluon distribution only enters indirectly at NLO, and is therefore much less well determined. Essentially the only constraint is the momentum sum rule, which shows that the gluon carries just less than 50% of the proton's momentum at $Q^2 \sim 4$ GeV^2. On the other hand, the gluon enters at *leading* order in large-p_T prompt photon production in hadron-hadron collisions: for $pp \to \gamma X$, the dominant QCD subprocess is $gq \to \gamma q$, in contrast to $p\bar{p} \to \gamma X$ where the annihilation process $q\bar{q} \to \gamma g$ is much more important. Particularly useful are data from the WA70 collaboration [12], which determine the gluon in the region $x \sim 0.35$. Combined with the momentum sum rule constraint, this leads to an input gluon behaviour proportional to $(1-x)^{5.3}$ at large x. The Drell-Yan $pN \to \mu^+\mu^- X$ process, which is mediated at leading order by $q_{\rm val}\bar{q}_{\rm sea} \to \gamma^*$, constrains the large-$x$ $(1-x)^{ns}$ behaviour of the sea quark distributions. The most precise data here are from the E605 collaboration [13]. Finally, data on W and Z production at $\bar{p}p$ colliders [14, 15] provide additional constraints on the u and d distributions, particularly when the accurate NMC measurements of $F_2^{\mu n}/F_2^{\mu p}$ are fitted simultaneously. Other hadron collider data, in particular on inclusive jet, prompt photon and $b\bar{b}$ production, provide important cross-checks on the gluon distribution, while not yet being of sufficient precision to influence the fits [16].

In the following section we describe in detail the theoretical framework used in the MRS parton distribution analysis. In subsequent sections we address two topical issues which impinge directly on the fits: the flavour structure of the quark sea and

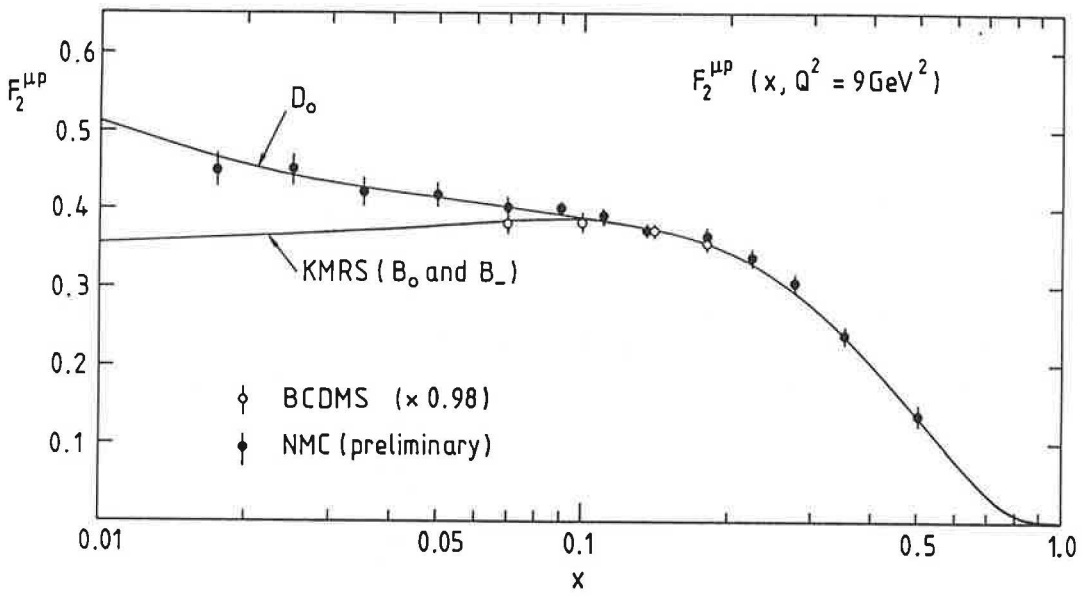

Figure 1: The structure function $F_2^{\mu p}(x, Q^2)$ as a function of x at $Q^2 = 9$ GeV^2 obtained by interpolating the measurements of the BCDMS collaboration [8] and preliminary measurements from NMC [9]. The upper curve corresponds to the D_0 set of partons [6], and the lower curve to the earlier KMRS sets of partons [5] obtained before the NMC data were available.

the form of the distributions at very small x. In Section 4 we compare our predictions at small x with the new data on F_2^{ep} from HERA.

2 The MRS(1992) analysis

Table 1 shows that the parton distributions f_i are determined from global fits to a wide range of deep-inelastic and related data. The basic procedure is to parametrize the f_i at a sufficiently large Q_0^2, (4 GeV^2 in the MRS analyses), so that $f_i(x, Q^2)$ can be calculated at higher Q^2 in perturbative QCD via the next-to-leading order (NLO) DGLAP evolution equations. In view of the quantity and variety of data to be fitted, it is remarkable that the starting distributions at Q_0^2 can be described by very simple parametrizations; in total only about 15 parameters are required. For the recent (S_0',D_0',D_-') sets we use

$$\begin{aligned} x\,[u_V + d_V] &= A_{ud}\, x^{\eta_1}\,(1-x)^{\eta_2}\,(1+\epsilon_{ud}\sqrt{x}+\gamma_{ud}x) \\ x\,d_V &= A_d\, x^{\eta_3}\,(1-x)^{\eta_4}\,(1+\epsilon_d\sqrt{x}+\gamma_d x) \\ x\,S &= A_S\, x^{\delta_g}\,(1-x)^{\eta_S}\,(1+\epsilon_S\sqrt{x}+\gamma_S x) \\ x\,g &= A_g\, x^{\delta_g}\,(1-x)^{\eta_g}\,(1+\gamma_g x)\,. \end{aligned} \qquad (2)$$

The flavour structure of the quark sea is

$$\begin{aligned} 2\,\bar{u} &= 0.4\,S - \Delta \\ 2\,\bar{d} &= 0.4\,S + \Delta \\ 2\,\bar{s} &= 0.2\,S \\ x\,\Delta &= A_\Delta\, x^{\eta_1}\,(1-x)^{\eta_S} \\ h &= 0, \quad Q^2 \leq 4m_h^2 \quad \text{for } h = c, b, \ldots\ . \end{aligned} \tag{3}$$

The numerical values of the parameters are listed in Table 2. Note that the distributions are defined in the $\overline{\rm MS}$ renormalization and factorization scheme. The fitted value of the QCD scale parameter is $\Lambda^{(4)}_{\overline{\rm MS}} = 230$ MeV ($\alpha_s(M_Z^2) = 0.112_5$), consistent with what is found by the experimental collaborations in fits to their own DIS data sets.

		S_0'	D_0'	D_-'	H
	(A_g)	2.78	2.78	0.338	0.787
Glue	δ_g	0	0	−0.5	−0.3
	η_g	5.3	5.3	5.3	5.3
	γ_g	0	0	10.6	5.20
	η_1	0.31	0.42	0.42	0.33
	η_2	3.85	3.92	3.92	3.89
	ϵ_{ud}	6.12	2.31	2.59	5.06
Valence	γ_{ud}	9.86	4.43	4.21	8.80
	η_3	0.82	0.24	0.24	0.22
	η_4	4.60	4.67	4.67	4.64
	ϵ_d	−1.38	43.3	28.7	101.
	γ_d	1.10	7.62	8.58	5.31
	A_S	1.98	2.03	0.083	0.386
	η_S	10	10	7.4	9.0
Sea	ϵ_S	−2.68	−2.98	8.57	0.013
	γ_S	7.98	8.47	15.8	12.0
	A_Δ	0	0.152	0.164	0.05

Table 2: Numerical values of the starting distribution parameters in the latest MRS(1992) fits. Note that A_g is fixed by the momentum sum rule, and is therefore not a free parameter.

Figures showing fits to all the input data and tables of the corresponding values of χ^2 can be found in Refs. [6, 7] and will not be presented again here. An example of the quality of the fit to the high precision muon deep-inelastic data has already been shown in Fig. 1. Figure 2 [7] shows the corresponding fit to the neutrino scattering data from CCFR [10]. Note that the data have been rescaled by a constant factor 0.95 (the normalization of the NMC data is taken as standard and other DIS sets are rescaled to give the best overall fit) and corrected for the effect of the heavy nuclear

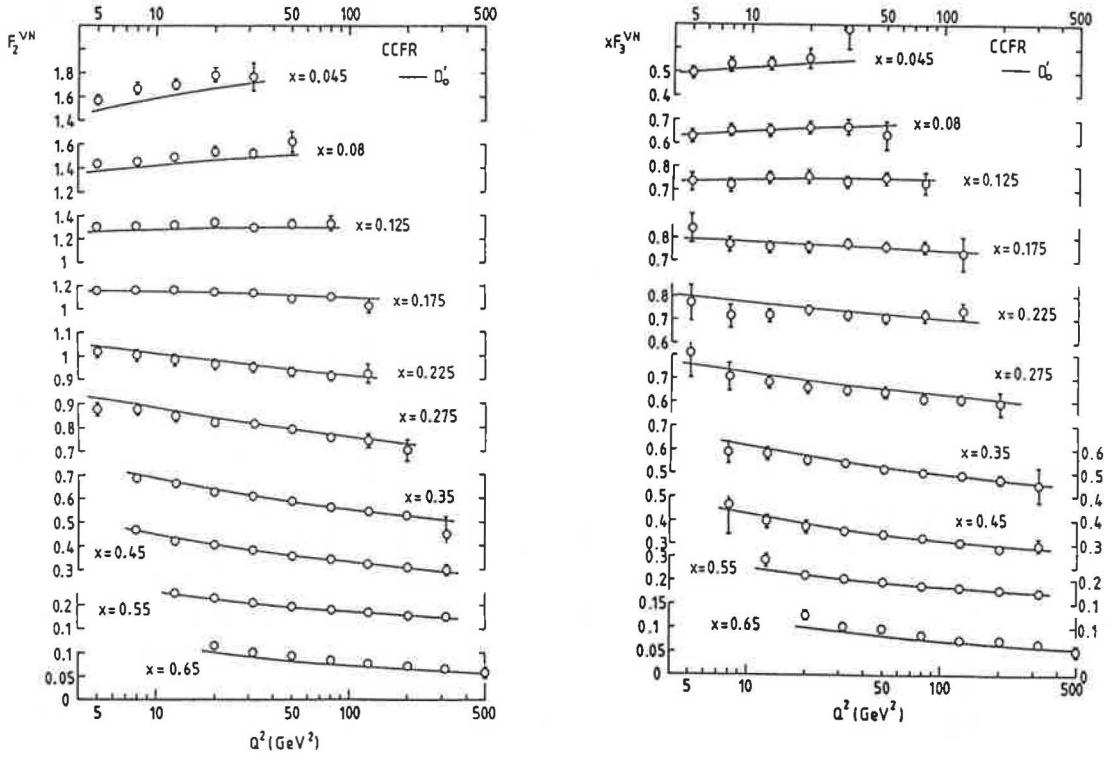

Figure 2: The $F_2^{\nu N}(x, Q^2)$ structure function measured by the CCFR collaboration [10]. The data are shown after correction for the heavy target effects and after an overall renormalization of 0.95 required by the global fit. The statistical, systematic and heavy target correction errors have been combined in quadrature. The curves correspond to the D_0' fit [7].

target [6]. To parametrize the uncertainty in this, a theory error of $\pm 2\%$ is included in the errors on the data shown in Fig. 2.

A key feature of the MRS analysis is that the parametrization of the starting distributions is designed not only to be 'minimal', in that extra parameters are included only when required by the data, but also to allow a clear picture of the underlying *physics* as revealed in the distributions. For example, the large-x behaviour of the various distributions (controlled by the parameters η_2, η_4, η_S and η_g) can be compared directly with predictions from dimensional counting, while the small-x behaviour (η_1, η_3 and δ_g) can be compared with the predictions of resummed perturbation theory and Regge theory.

3 Flavour structure of the quark sea

3.1 Up-down flavour asymmetry

It is difficult to determine $\bar{u}$ and $\bar{d}$ separately from the deep-inelastic data. In fact, prior to 1992 most analyses assumed that the non-strange sea was flavour symmetric, *i.e.* $\bar{u} = \bar{d}$. The motivation for allowing $\bar{u} \neq \bar{d}$ came from comparing the NMC

measurement [11] of the Gottfried Sum

$$\int_{0.004}^{0.8} \frac{dx}{x} (F_2^{\mu p} - F_2^{\mu n}) = 0.227 \pm 0.007\,(\text{stat.}) \pm 0.014\,(\text{sys.}) \qquad (4)$$

at $Q^2 = 4$ GeV^2 with the theoretical expectation

$$I_{\text{GSR}} = \int_0^1 \frac{dx}{x} (F_2^{\mu p} - F_2^{\mu n}) = \tfrac{1}{3}\int_0^1 \frac{dx}{x} (u_V - d_V) + \tfrac{2}{3}\int_0^1 \frac{dx}{x} (\bar{u} - \bar{d})$$
$$= \tfrac{1}{3}, \quad \text{if } \bar{u} = \bar{d}\,. \qquad (5)$$

A straightforward comparison of (4) and (5) implies $\bar{u} \neq \bar{d}$. In the MRS 'D' fits [6, 7] $\bar{d} - \bar{u}$ is parametrized according to (3), with the parameter A_Δ chosen such that the measured value of I_{GSR} is reproduced. It is interesting to note, however, that even including the NMC data it is still possible to maintain $\bar{u} = \bar{d}$ and obtain an equally good global description of the data, at the expense of a contrived small-x behaviour of the valence distributions, as in set S_0 [6] or S_0' [7]. On the other hand, the lack of Regge $\rho - a_2$ exchange degeneracy suggests that it is more reasonable to allow $\bar{u} \neq \bar{d}$, as in sets D_0' and D_-'. The fits to the NMC data on $F_2^{\mu p} - F_2^{\mu n}$ are shown in Fig. 3.‡

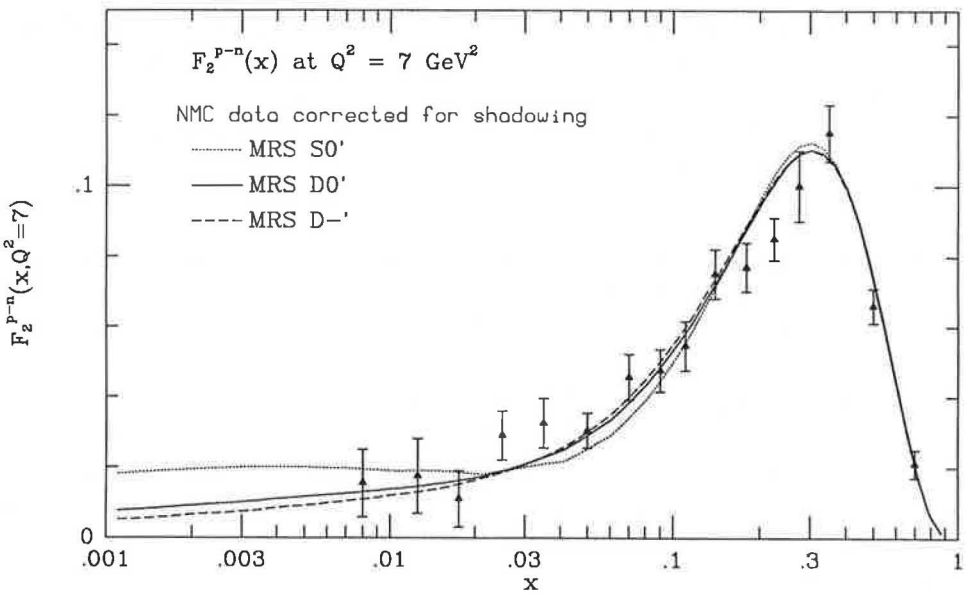

Figure 3: The structure function difference $F_2^{\mu p} - F_2^{\mu n}$ from NMC [11], with the $((S_0', D_0', D_-')$ fits [18].

The detailed structure of $\bar{d} - \bar{u}$ is not determined by the available DIS data. All we really know is that on average $\bar{d} > \bar{u}$ at small x. An independent method for

‡Note that the latest MRS(D_0',D_-',H) sets have $I_{\text{GSR}} = 0.256, 0.240, 0.290$. An updated analysis of the Gottfried Sum by NMC gives $I_{\text{GSR}} = 0.258 \pm 0.010(\text{stat.}) \pm 0.015(\text{sys.})$ at $Q^2 = 4$ GeV^2 [17].

obtaining further information on $\bar{d} - \bar{u}$ [19] is to compare (Drell-Yan) lepton-pair production in pp and pn collisions, via the asymmetry

$$A_{\rm DY} \;=\; \frac{\sigma_{pp} - \sigma_{pn}}{\sigma_{pp} + \sigma_{pn}} \,. \tag{6}$$

Because $u > d$ in the proton, the asymmetry is positive for sets with $\bar{d} - \bar{u}$ zero or small at large x. A measurement [20] of the asymmetry to an accuracy of a few per cent will provide a powerful discriminator of the possible behaviours of $\bar{d} - \bar{u}$. Predictions of various sets of parton distributions and a more complete discussion can be found in Ref. [18].

3.2 Strange quarks

The strange quark distribution can be extracted directly from accurate measurements of the *difference* between the F_2 structure functions measured in neutrino scattering off a heavy isoscalar target and muon scattering off a deuterium target:

$$xs(x) \;=\; \tfrac{5}{6}\, F_2^{\nu N}(x) \;-\; 3\, F_2^{\mu D}(x) \,. \tag{7}$$

This method for obtaining $s(x)$ is, however, subject to considerable uncertainties. It relies on an accurate knowledge of the structure function normalization in the two types of experiment and, in the case of neutrino scattering, is sensitive to the heavy target corrections used. A more reliable method is to use the presence of an extra muon in deep-inelastic neutrino scattering to tag events originating in $sW^+ \to c(\to \mu^+ + \ldots)$, *i.e.*

$$\sigma(\nu N \to \mu^- \mu^+ + \ldots) \;\propto\; \{(u+d)|V_{cd}|^2 + 2s|V_{cs}|^2\}\, D^{c\to\mu^+} \;\simeq\; 2s|V_{cs}|^2\, D^{c\to\mu^+} \,. \tag{8}$$

Early measurements of the dimuon rate were, in fact, the motivation for the 50% suppression of the strange quarks in the MRS analyses, see Eq. (3). By utilizing both neutrino and antineutrino scattering it is possible to measure this suppression directly, through the ratio $\kappa = 2\int s/(\int \bar{u} + \int \bar{d})$ where $\int s \equiv \int_0^1 s(x)dx$ *etc.* A recent next-to-leading order QCD analysis by the CCFR collaboration [21] gives

$$\kappa \;=\; 0.435 \;\pm 0.058\,(\text{stat.}) \;\pm 0.012\,(\text{sys.}) \,. \tag{9}$$

This result is in almost perfect agreement with the MRS predictions. Figure 4 shows the strange quark distribution extracted by CCFR at $Q^2 = 4$ GeV^2 (in the form of a '1σ' band of distributions) together with the MRS($\rm D_0'$,$\rm D_-'$) predictions [7].

Figure 4 also shows the predictions of set 1M from the recent CTEQ analysis [23]. This has a much larger strange sea and is clearly disfavoured by the dimuon data. The reason lies in the different treatment of the sea quark distributions in the two analyses. In contrast to MRS, the CTEQ sea distributions are freely and independently parametrized, with no *ab initio* strange suppression. The large strange sea originates from their simultaneous fit to the F_2 structure functions, which essentially corresponds to using Eq. (7). There *is* a slight disagreement between the MRS

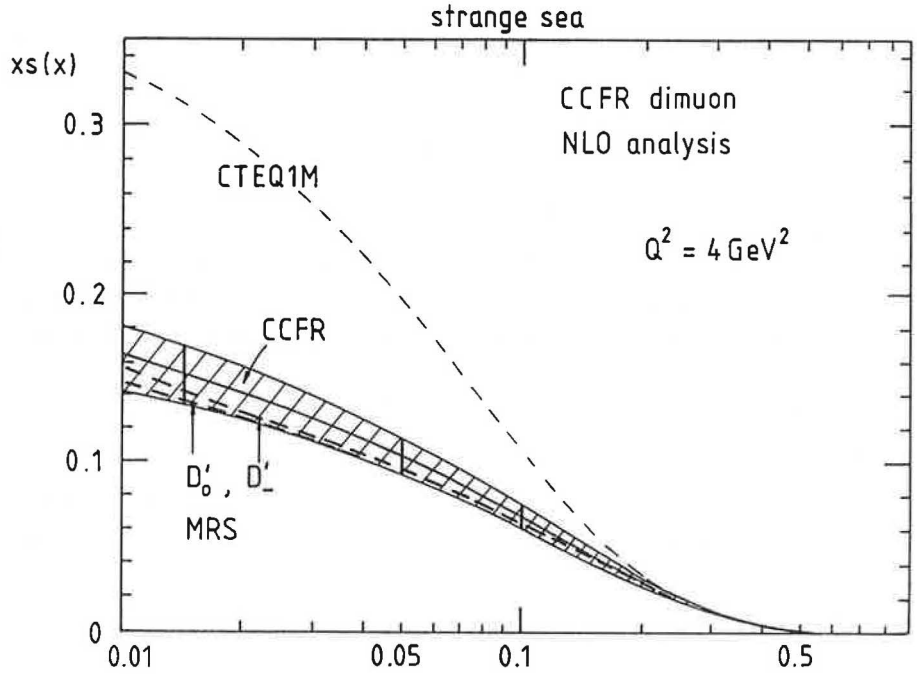

Figure 4: The strange quark distribution (shaded band) at $Q^2 = 4$ GeV^2 as extracted from the dimuon cross section using a next-to-leading order QCD analysis, from the CCFR collaboration [21]. Also shown are the MRS(D_0',D_-') [7] and the CTEQ [23] predictions.

fits and the $F_2^{\nu N}$ data at small x, see Fig. 2, although not as large as the size of the CTEQ strange sea would suggest. The reason is that in the MRS analysis, the CCFR data are renormalized by 0.95 relative to the NMC data, and allowance is made in the neutrino data errors for the uncertainty in the heavy target correction [22]. It is interesting to speculate whether the slight disagreement evident at small x in Fig. 2 is due to some experimental problem or whether, as argued for example in Ref. [25], there *should* be some difference in the strange sea as measured in neutrino and muon scattering. Such a difference could result, for example, from the different mass thresholds involved in the two types of scattering, $W^+g \to c\bar{s}$ *vs.* $\gamma^*g \to s\bar{s}$, if the heavy flavours are assumed to originate in gluon splitting.

4 Parton distributions at small x

In the MRS fits, the small-x form of the gluon and sea-quark distributions at Q_0^2 is fixed at either $xf \sim x^0$ or $xf \sim x^{-1/2}$. These represent two 'extreme' forms of theoretical behaviour: x^0 is the standard non-perturbative Regge prediction, based on the high energy behaviour of the photon-quark forward scattering amplitude:

$$\lim_{\nu\to\infty} \mathrm{Im}\, A(\gamma q \to \gamma q) \sim \nu^{\alpha_P} \Rightarrow \lim_{x\to 0} F_2 \sim x^{1-\alpha_P} \,. \qquad (10)$$

Assuming Pomeron exchange dominance gives $\alpha_P \simeq 1$ and therefore $xf \sim x^0$. It is likely, however, that in practice the more dominant effect at small x comes from perturbatively calculable multiple soft-gluon emission, as embodied in the 'Lipatov' (or BFKL) equation [1]. The k_T differential distribution, defined by

$$xg(x,Q^2) = \int^{Q^2} \frac{dk_T^2}{k_T^2} f(x,k_T^2) \tag{11}$$

satisfies an evolution equation in $\log(1/x)$,

$$-x\frac{\partial f}{\partial x} = \int dk'^2 K(k,k') f(x,k'^2)\ , \tag{12}$$

and the small-x behaviour is controlled by the largest eigenvalue λ of the eigenfunction equation $K \otimes f_n = \lambda_n f_n$, for then $f \sim \exp(\lambda \log(1/x)) \sim x^{-\lambda}$ as $x \to 0$. For fixed strong coupling $\lambda = 4C_A(\log 2)\,\alpha_s/\pi \approx 0.5$, which gives the small-$x$ behaviour assumed for the set D$'_-$.

It should be stressed, however, that this is a leading-logarithm, fixed-coupling prediction—it is not yet known if the $x^{-1/2}$ behaviour survives a proper treatment of subleading effects, for example, from next-to-leading logarithms, infra-red cut-offs, parton saturation, kinematic constraints *etc.* It is likely that the net effect of these is to slow down the growth of the distributions at small x, see for example Ref. [24].

The predictions of the MRS(D$'_0$,D$'_-$) sets for F_2^{ep} in the small-x HERA regime are shown in Fig. 5. Note that the predictions are essentially identical for $x \gtrsim 0.02$ (the fixed target DIS data are equally well fitted by both sets) but, by construction, are dramatically different at small x. Also shown are (i) the CTEQ1M and CTEQ1MS predictions [23] and (ii) the predictions from the 'dynamical quark' model of Glück, Reya and Vogt (GRV) [26]. For the former analysis, the small x behaviour is essentially determined by the lowest x points of the fixed-target DIS data, with no particular theoretical constraints imposed. In the latter approach, 'valence-like' distributions at very low Q ($Q_0^2 = 0.3$ GeV^2) are evolved and fitted to MRS valence quark distributions at a higher Q. The growth seen for GRV at small x is thus a result of perturbative DGLAP Q^2 evolution. By coincidence, it is not unlike that seen for D$'_-$, at least in the HERA regime.

5 First results from HERA

The new results on F_2 from the H1 [27] and ZEUS [28] collaborations confirm the dramatic behaviour first evident in the preliminary data analysis—the structure function rises at small x, in line with the expected Lipatov behaviour. This is illustrated in Fig. 6, which shows the new data together with the MRS(D$'_0$,D$'_-$) predictions. The data clearly prefer the D$'_-$ prediction.[§] The errorbars are still too large to make a truly quantitative comparison: one would like, for example, to see whether the data favoured a pure $x^{-\lambda}$ form over the more complicated form of the dynamical quark

[§]Note that the Q^2 dependence is also consistent, within large errors, with DGLAP evolution.

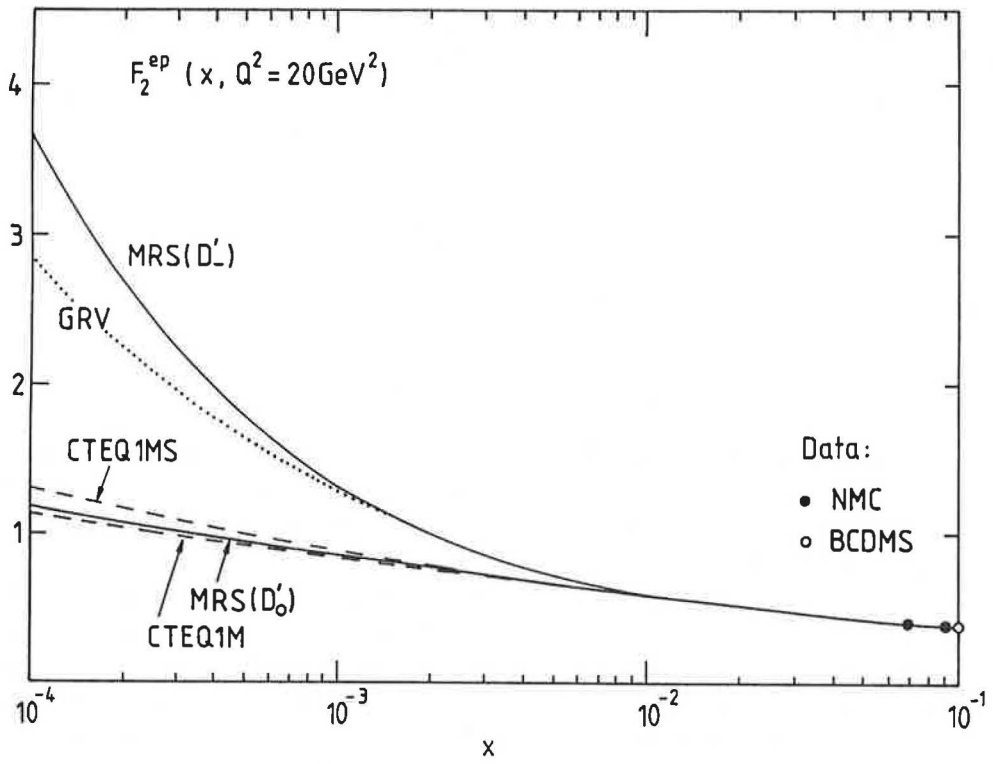

Figure 5: Predictions for F_2^{ep} at $Q^2 = 20$ GeV^2 obtained from the parton sets from Refs. [7, 23, 26].

model [26]. In the meantime, it is straightforward to 'tune' the exponent δ_g of the input sea and gluon distributions (Eq. (2)) to obtain a best fit to the new data. The result of doing this – set MRS(H) with $\delta_g = -0.3$ – is shown as the dotted curve in Fig. 6. The other parameters for this new fit are listed in Table 2.

The measurements of F_2^{ep} at HERA probe primarily the sea quark distribution at small x. If the 'perturbative pomeron' is indeed responsible for the steep rise, then the same behaviour should also be seen in the gluon distribution. Methods for directly extracting the gluon distribution from HERA measurements of the longitudinal structure function F_L [29] and $dF_2/d\log Q^2$ have been suggested. These are based on the observation that in the leading-order expressions

$$\begin{aligned} F_L(x,Q^2) &= \frac{\alpha_s(Q^2)}{\pi}\left\{\frac{4}{3}\int_x^1 \frac{dy}{y}\left(\frac{x}{y}\right)^2 F_2(y,Q^2)\right. \\ &\quad \left. +2\sum_q e_q^2 \int_x^1 \frac{dy}{y}\left(\frac{x}{y}\right)^2\left(1-\frac{x}{y}\right) yg(y,Q^2)\right\} \qquad (13) \\ \frac{dF_2(x,Q^2)}{d\log Q^2} &= \frac{\alpha_s(Q^2)}{2\pi}\left\{\int_x^1 \frac{dy}{y}\left(\frac{x}{y}\right) P_{qq}\left(\frac{x}{y}\right) F_2(y,Q^2)\right. \end{aligned}$$

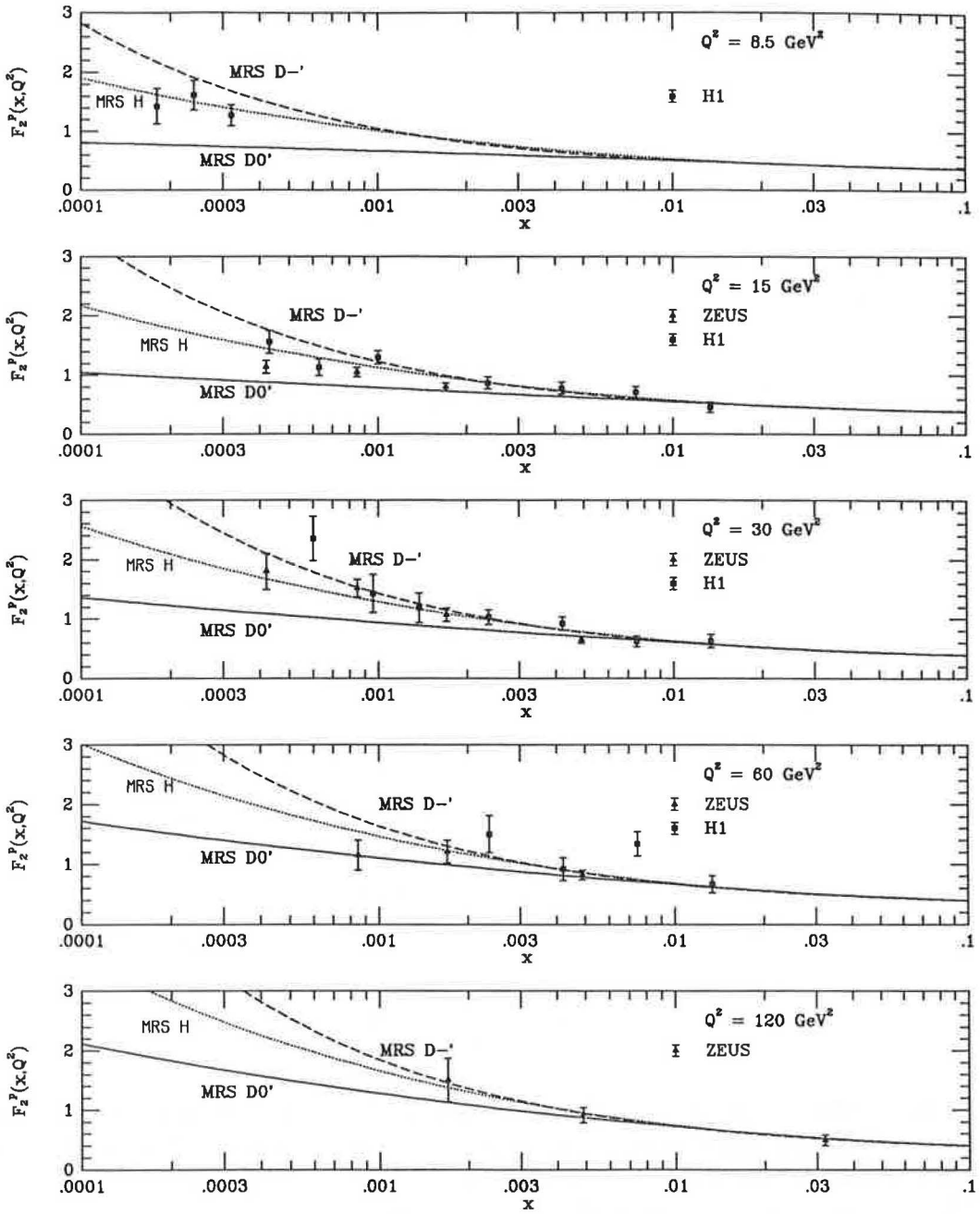

Figure 6: The structure function F_2^{ep} from H1 [27] and ZEUS [28] at HERA, with the predictions from the MRS parton sets D_0' and D_-' [7]. Also shown is a new fit MRS(H) with $\delta_g = -0.3$, which minimizes the overall χ^2.

$$+2\sum_q e_q^2 \int_x^1 \frac{dy}{y}\left(\frac{x}{y}\right) P_{qg}\left(\frac{x}{y}\right) yg(y,Q^2)\Bigg\} \qquad (14)$$

it is the gluon term on the right-hand-side that dominates at small x in each case. The predictions of the MRS(D_0',D_-') sets for these two quantities are shown, with the gluon distributions, in Fig. 7. The clear correlations lend support to the case for

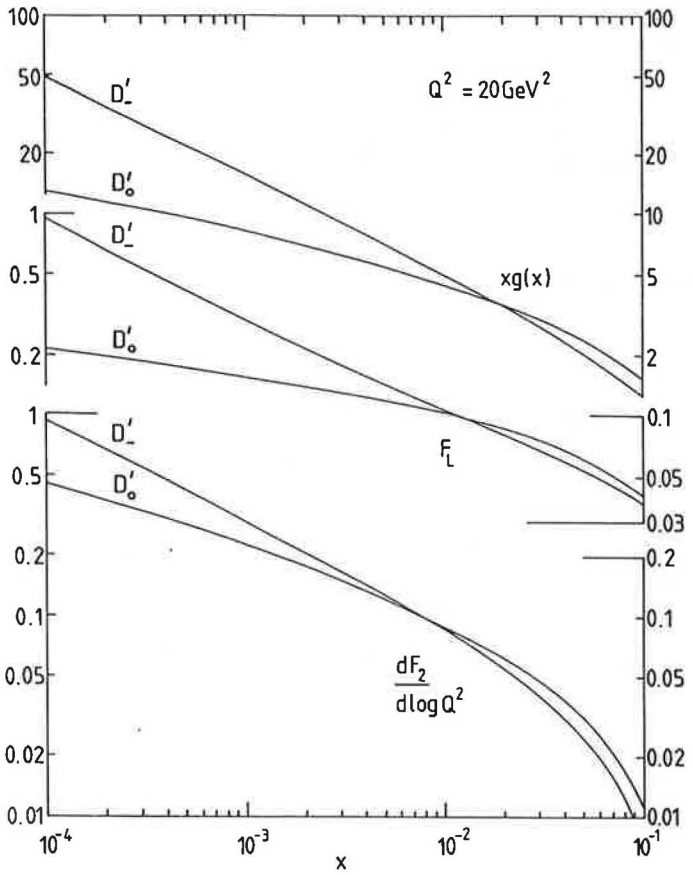

Figure 7: The sensitivity of two structure function methods of determining the small x gluon at HERA, illustrated in terms of the gluon distributions of [7]. F_L is the longitudinal structure function for deep-inelastic ep scattering. The curves are calculated using the full next-to-leading order QCD expressions.

making precise measurements of these two quantities, leading to qualitative estimates of the underlying gluon behaviour.

Finally, we can ask whether any further information on the small x partons can be obtained from hadron colliders, in particular that Fermilab $p\bar{p}$ collider. It is straightforward to show that at $\sqrt{s} = 1.8$ TeV, x values comparable to those currently measured at HERA can be probed either by very small mass systems produced

centrally, or by more massive final states at large rapidity. The Drell-Yan process offers some possibilities for the former (see for example Ref. [30]) while 'medium-p_T' forward jet production is ideal for the latter. As an illustration, Fig. 8 shows the ratio of same-side to opposite-side jet cross sections from CDF [31], as a function of the equal and opposite jet rapidities y. The curves are the MRS(D_0',D_-') predictions evaluated at leading order with a renormalization/factorization scale chosen to mimic the NLO corrections. Further details of this analysis can be found in Ref. [32]. At large rapidity, the ratio is sensitive to the small-x *gluon* distribution, and it is interesting to note that, despite the uncertainties from both theory and experiment, once again the D_-' prediction is preferred.

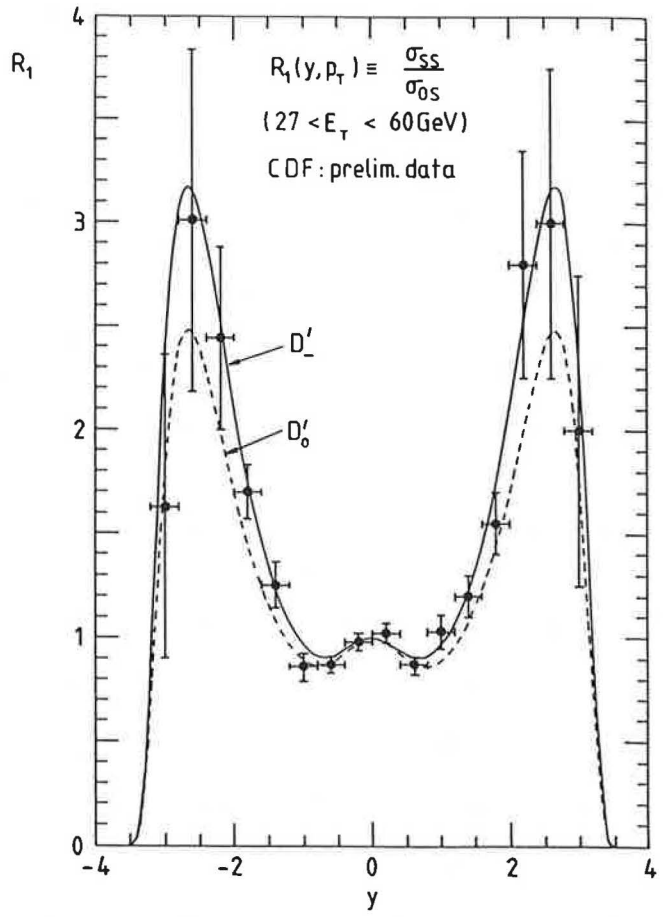

Figure 8: The curves show the same-side/opposite-side dijet ratio predictions from the D_-' and D_0' partons [7], for $27 < p_T < 60$ GeV. The data points are the preliminary CDF measurements [31], but note that the measured jet p_T values have not been corrected for CDF detector effects and therefore do not correspond directly to the true jet transverse energies.

6 Outlook

The structure function data from HERA shown in the previous section is based on only about 25 nb^{-1} at each detector, accumulated during 1992. Since the corresponding integrated luminosity is already close to 500 nb^{-1}, it is clear that our knowledge of the small-x region will be significantly improved over the next year. The increased precision of the gluon and sea distributions will not only shed light on the topical question of the dynamics of perturbative QCD at low x, but will also allow the predictions for many processes at LHC and SSC to be sharpened. Continuing to improve our knowledge of the partonic structure of the proton will clearly be a high priority for some time to come.

References

[1] E.A. Kuraev, L.N. Lipatov and V.S. Fadin, Sov. Phys. JETP **45** (1977) 199. Ya.Ya. Balitsky and L.N. Lipatov, Sov. J. Nucl. Phys. **28** (1978) 822.

[2] *PDFLIB: A library of all available parton density functions of the nucleon, the pion and the photon and the corresponding α_s calculations*, H. Plothow-Besch, Comp. Phys. Commun. **75** (1993) 396.

[3] A.D. Martin, R.G. Roberts and W.J. Stirling, Phys. Rev. **D37** (1988) 1161; see also Phys. Lett. **206B** (1988) 327; Mod. Phys. Lett. **A4** (1989) 1135.

[4] P.N. Harriman, A.D. Martin, R.G. Roberts and W.J. Stirling, Phys. Rev. **D42** (1990) 798.

[5] J. Kwiecinski, A.D. Martin, R.G Roberts and W.J. Stirling, Phys. Rev. **D42** (1990) 3645.

[6] A.D. Martin, W.J. Stirling and R.G. Roberts, Phys. Rev. **D47** (1993) 867.

[7] A.D. Martin, W.J. Stirling and R.G. Roberts, Phys. Lett. **306B** (1993) 145.

[8] BCDMS collaboration: A.C. Benvenuti *et al.*, Phys. Lett. **223B** (1989) 485.

[9] NMC: P. Amaudruz *et al.*, Phys. Lett. **295B** (1992) 159.

[10] CCFR collaboration: Phys. Rev. Lett., to be published.

[11] NMC: P. Amaudruz *et al.*, Phys. Rev. Lett. **66** (1991) 2712; E.M. Kabuß, Nucl. Phys. B (Proc. Supp.) **29A** (1992) 1.

[12] WA70 collaboration: M. Bonesini *et al.*, Z. Phys. **C38** (1988) 371.

[13] E605 collaboration: C.N. Brown *et al.*, Phys. Rev. Lett. **63** (1989) 2637.

[14] UA2 collaboration: J. Alitti *et al.*, Phys. Lett. **276B** (1992) 365.

[15] CDF collaboration: F. Abe *et al.*, Phys. Rev. **D44** (1991) 29.

[16] See for example: W.J. Stirling, Proc. Conf. on 'QCD – 20 Years Later', Aachen, eds. P.M. Zerwas and H.A. Kastrup, World Scientific, Vol.1, p.387 (1993).

[17] NMC: M. Arneodo *et al.*, preprint CERN-PPE/93-117 (1993).

[18] A.D. Martin, R.G. Roberts and W.J. Stirling, Phys. Lett. **B308** (1993) 377.

[19] S.D. Ellis and W.J. Stirling, Phys. Lett. **B256** (1991) 258.

[20] M.C. Abreu *et al.*, CERN proposal SPSLC 92-15 (1992).
G.T. Garvey *et al.*, Fermilab proposal P866 (1992).

[21] CCFR collaboration: A. Bazarko *et al.*, Columbia University preprint NEVIS–1492 (1993).

[22] A.D. Martin, R.G. Roberts and W.J. Stirling, 'Present status of parton distributions', Proc. of the Durham Workshop on 'HERA – the new frontier for QCD', to be published in J. Phys. **G**, RAL preprint RAL-93-027 (1993).

[23] CTEQ collaboration: J. Botts, J. Morfin, J. Owens, J. Qiu, W.-K. Tung and H. Weerts, Phys. Lett. **304B** (1993) 159.

[24] A.J. Askew, J. Kwiecinski, A.D. Martin and P.J. Sutton, Phys. Rev. **D47** (1993) 3775.

[25] V. Barone *et al.*, Phys. Lett. **B268** (1991) 279; University of Turin preprints DFTT-28/93, DFTT-39/93 (1993).

[26] M. Glück, E. Reya and A. Vogt, Z. Phys. **C48** (1990) 471, **C53** (1992) 127; Phys. Lett. **B306** (1993) 391.

[27] H1 collaboration: I. Abt *et al.*, preprint DESY-93-117 (August 1993).

[28] ZEUS collaboration: M. Derrick *et al.*, preprint DESY-93-110 (August 1993).

[29] A.M. Cooper-Sarkar *et al.*, Zeit. Phys. **C39** (1988) 281.

[30] CDF collaboration: F. Abe *et al.*, preprint FERMILAB-PUB-93-133-E (1993).

[31] CDF collaboration: contribution to the EPS Conference on High Energy Physics, Marseilles, July 1993, preprint FERMILAB-Conf-93/203-E (1993).

[32] A.D. Martin, R.G. Roberts and W.J. Stirling, University of Durham preprint DTP/93/48 (1993).